Welding in the World (2025) 69:739–750
https://doi.org/10.1007/s40194-024-01890-7

RESEARCH PAPER

Significance of fracture toughness for linear friction welded joint of weathering steel

Kazuma Shimizu[1] · Shota Nakayama[1] · Hiroto Shoji[1] · Takumi Kawakubo[2] · Tomoya Nagira[3] · Mitsuru Ohata[1] · Hidetoshi Fujii[2]

Received: 16 May 2024 / Accepted: 15 November 2024 / Published online: 26 December 2024

Abstract
This paper examined the characteristics and significance of fracture toughness for LFW (linear friction welding) joints of weathering steel SPA-H processed under different joining conditions to control maximum temperature during LFW process. Two types of LFW joint were prepared; one was jointed under higher compressive pressure so as a maximum temperature during LFW process to be lower than the A_1-transformation temperature (A1-LFW), and the other was jointed under lower compressive pressure to be higher than the A_3-transformation temperature (A3-LFW). The fracture toughness of both joints where a crack was located at the joint interface exhibited a higher value than that of the heat-affected zone of MAG (metal active gas) welds for the same steel. These results indicated that the LFW was more effective for the joining of weathering steel compared with conventional arc welding in terms of fracture toughness. However, A1-LFW exhibited lower fracture toughness (critical CTOD) than that of base metal or A3-LFW. Thus, the significance of the test results was discussed from mechanical and metallurgical viewpoints. The fracture toughness for A1-LFW found to be deteriorated due to work hardening associated with compressive plastic straining during LFW under higher compressive pressure, where the metal heated under A_1-temperature was not completely ejected by friction but remained around the joint interface. On the other hand, the deterioration of fracture toughness for A3-LFW was found to be caused by hardening due to bainitic transformation near the joint interface, whereas the narrowness of the hardened region provided a little bit higher toughness than the intrinsic toughness of the transformed phase due to plastic constraint loss.

Keywords Linear friction weld · Fracture toughness · Plastic constraint · Strength mismatch

1 Introduction

Linear friction welding (LFW) is one of the solid-state joining processes, which is achieved by oscillating two components relatively under a high contact load [1]. After LFW equipment was manufactured in The Welding Institute (TWI), LFW technique was developed with mainly focusing on aerospace-applied titanium and nickel alloys [2–4]. Recently, the preferable condition for LFW process from metallurgical viewpoints which enable lower temperature during LFW process was discovered [5, 6]. The theory could avoid mechanical property deterioration due to softening caused by high temperature for LFW of AA7075-T6 alloy [7]. By using this theory, the temperature during LFW process could be lower than the melting point or transformation point of steel so that the material deterioration due to the high temperature during fusion welding can be improved. Therefore, LFW process is also expected to be the alternative joining method of low-weldability metals like weathering steel, which is used in structural components.

In the view of structural stability of fracture, several studies have been conducted on the fracture of LFW joints [8–12]. Some of the studies focused on the crack growth from the weld toe part where stress concentration occurred

Recommended for publication by Commission X - Structural Performances of Welded Joints - Fracture Avoidance

✉ Kazuma Shimizu
k.shimizu@mapse.eng.osaka-u.ac.jp

[1] Graduate School of Engineering, Osaka University, Suita, Osaka, Japan

[2] Joining and Welding Research Institute, Osaka University, Ibaragi, Osaka, Japan

[3] National Institute for Materials Science, Tsukuba, Ibaraki, Japan

Table 1 Chemical composition (mass %) of base steel

SPA-H mass (%)	C	Si	Mn	P	S	Cu	Ni	Cr
	0.08	0.43	0.38	0.094	0.003	0.31	0.18	0.67

[8–11]. Assuming the unstable fracture after such fatigue crack growth, the brittle fracture resistance of the weld joint is also important. Some experiments have been conducted on the fracture toughness of LFW joints [12, 13]. These studies focused on the impact toughness and the fracture path under unstable ductile fracture of for Ti–6Al–4 V alloy LFW joint that has no concern of brittle fracture [12]. However, few reports have been conducted on the brittle fracture of cracked LFW joints of steel.

Generally, the fracture resistance of weld joints is dependent on the deterioration of the material at the crack-tip but also the difference in strength, that is called strength-mismatch [14–18]. In LFW process, the degree of strength-mismatch near the joining interface depends on material properties and joining conditions [7, 13]. In addition, the lack of bonding in the interface zone was concerned to be a crack-like defect [19]. To apply LFW process as a joining method in structural components made by low-weldability steel, it is essential to reveal the characteristic of fracture toughness of LFW joints in terms of not only material property but also strength-mismatch.

The purpose of this study is to reveal the characteristics and the significance for fracture toughness for LFW joints of weathering steel SPA-H processed under different joining conditions to control maximum temperature. The significance of fracture toughness is also discussed from mechanical and metallurgical viewpoints of the joints.

2 Fracture toughness testing of linear friction welded joint

In order to examine the effect of conditions to control maximum temperature during LFW process on the fracture toughness of weld joint, two types of joints, the maximum temperature during LFW process was lower or higher than the transformation temperature, were subjected to fracture toughness test. For comparison, CO_2 gas welded joint and base metal were also subjected to fracture toughness test.

The base material used was weathering steel, SPA-H. Tables 1 and 2 show the chemical composition and mechanical properties of the steel, respectively. Table 3 gives the conditions used for LFW process. Base steel plates with thickness $t = 3$ mm and width 30 mm were subjected to LFW process with applied pressure 250 MPa so as the maximum temperature to be lower than the A1-transformation temperature during LFW process (A1-LFW). On the other hand, plates with thickness $t = 12$ mm and width 30 mm were subjected to LFW process with applied pressure 50 MPa so as the maximum temperature to be higher than the A3-transformation temperature during LFW process (A3-LFW). The geometry of LFW joint for A1-LFW or A3-LFW is shown in Fig. 1. Plates with thickness $t = 12$ mm were also subjected to CO2 gas shielded welding, that is a kind of metal active gas welding process (MAG). The solid wire used was YM-55W (Nippon Steel Welding & Engineering CO., LTD). Table 4 gives conditions used for MAG welding process.

Table 2 Mechanical properties at R.T. of base steel

SPA-H at R.T	$\sigma_{0.2}$ (MPa)	σ_T (MPa)	YR (%)	ε_T (%)
	372	502	74.1	28.7

$\sigma_{0.2}$, 0.2% proof stress; σ_T, tensile strength; *YR*, yield-to-tensile ratio; ε_T, uniform elongation

Table 3 Conditions used for LFW-process

	Max. temperature	*P* (MPa)	*f* (Hz)	*A* (mm)
A1-LFW	Lower than A_1	250	15	1.5
A3-LFW	Higher than A_3	50		

A_1, A_1 transformation temperature (= 723 °C); A_3, A_3 transformation temperature (= 910 °C)

P, applied pressure; *f*, frequency; *A*, amplitude

In order to examine the fracture toughness of the joint for A1-LFW and A3-LFW, small-size 3-point bend (3 PB) specimens with an initial crack at the joint interface were subjected to fracture toughness testing. The position of specimen extraction is schematically shown in Fig. 2. From each mid-thickness position of A1-LFW with thickness $t = 3$ mm and A3-LFW with thickness $t = 12$ mm, 3 PB specimens with thickness $B = 3$ mm were extracted so as thickness through crack to be located at the joint interface. For comparison, 3 PB specimens were also extracted from MAG welds of for the same steel so as thickness through crack to be into HAZ (just next to FL). Configuration of the 3 PB specimen is shown in Fig. 3. The geometry of the 3 PB specimen was $B = 3$ mm (specimen thickness) $\times W = 6$ mm (specimen width), which is the symmetrically reduced geometry of the 3-point bend fracture toughness test specimen in accordance with ISO12135: 2021 [20].

The fracture toughness test was performed by using the testing machine designed for small-size specimens. An overview of the fracture toughness test is presented in Fig. 4. The 3 PB specimen was subjected to a fracture test at − 50

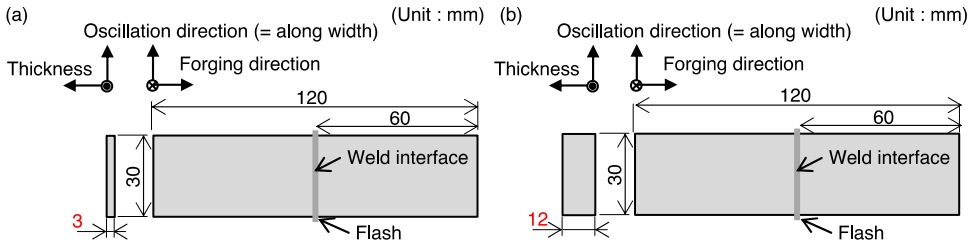

Fig. 1 Configuration of LFW joint used for fracture toughness test **a** A1-LFW and **b** A3-LFW

Table 4 Conditions used for metal active gas welding (MAG)

	Pass	Current (A)	Voltage (V)	Velocity (cm/min)
MAG	1	300	82	10

°C in a cooling bath filled with nitrogen-atmosphere. Test temperature was controlled by measuring the temperature on the surface of the specimen by using a thermocouple. Since the specimen was too small to install a clip-gauge, the crack mouth opening displacement V_g was measured by

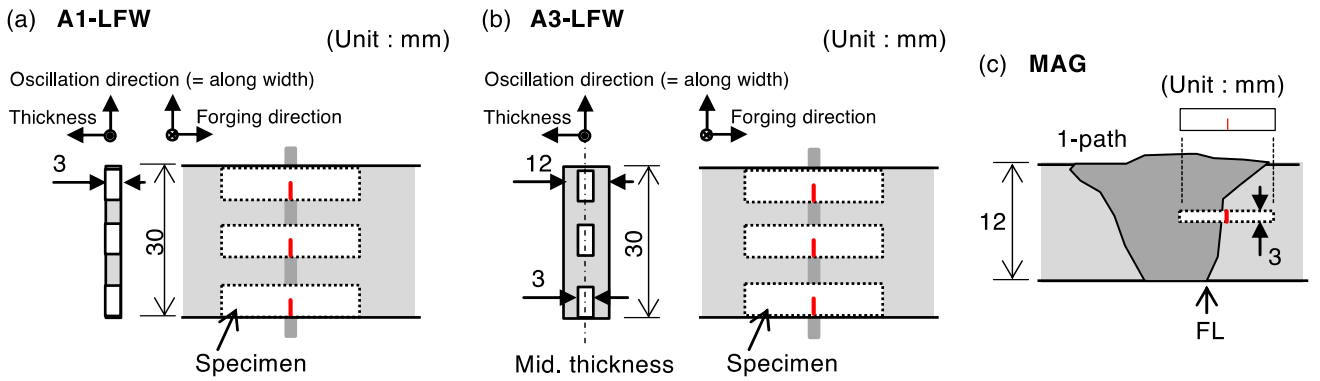

Fig. 2 Extraction of fracture toughness test specimen from joints **a** A1-LFW, **b** A3-LFW, and **c** MAG

Fig. 3 Configuration of 3 PB specimen used for fracture toughness test **a** overview and **b** detail around notch

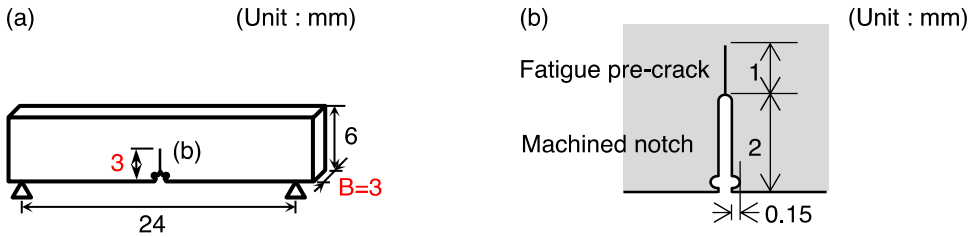

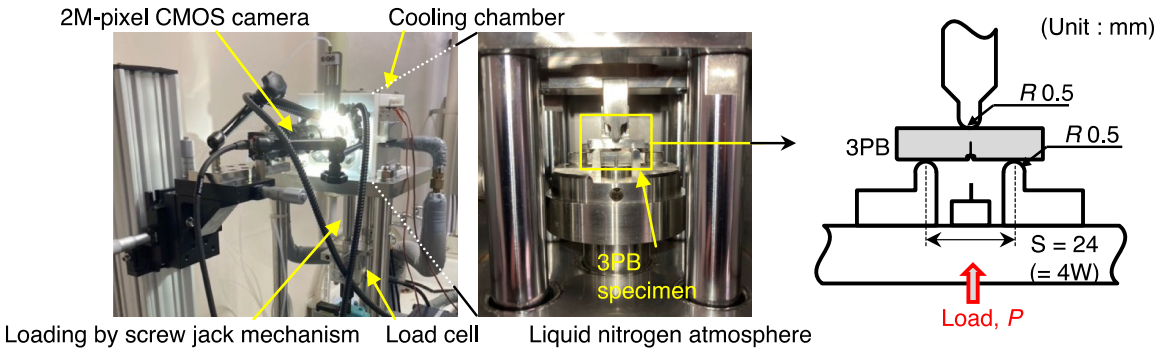

Fig. 4 3 PB testing machine for small specimen under low temperature

a non-contacting optical extensometer with real-time image processing. The critical CTOD was calculated according to the WES1108:2015 [21].

Figures 5 and 6 show the representative fracture appearance and critical CTOD obtained by the 3PB test, respectively. 2 of 4 specimens for A1-LFW, 2 of 6 specimens for A3-LFW, and 4 of 5 specimens for MAG fractured in a cleavage manner without ductile crack growth larger than 0.2 mm (critical CTOD for cleavage fracture, δ_c). Other specimens for A1-LFWs, A3-LFWs, MAG, and all specimens for BM achieved maximum load plateau without unstable fracture (CTOD at maximum load point, δ_m). Figure 6 compares critical CTOD for A1-LFW, A3-LFW, MAG-joint, and BM. LFW joint, both of A1-LFW and A3-LFW, exhibited higher critical CTOD than that of the heat-affected zone of MAG for the same steel. These results indicated that the LFW was more effective for the joining of weathering steel compared with conventional fusion welding in terms of fracture toughness. However, A1-LFW exhibited lower critical CTOD than that of base metal and A3-LFW.

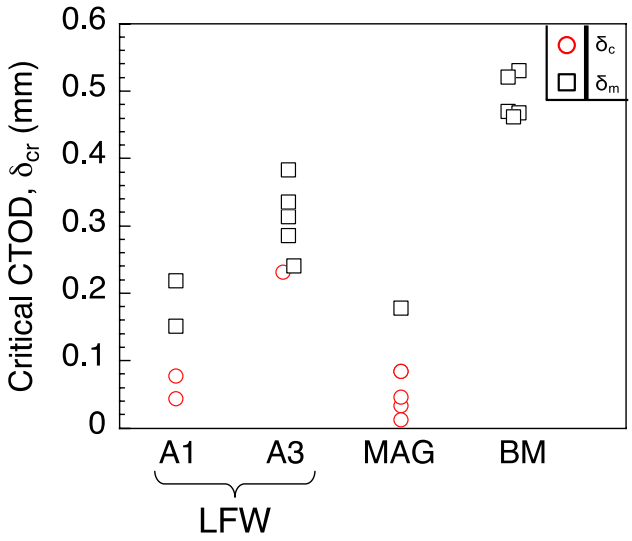

Fig. 6 Critical CTOD obtained by 3 PB test

3 Significance of fracture toughness from the mechanical aspect

This section concerns the significance of the fracture toughness of A1-LFW and A2-joint from mechanical viewpoints. The effect of strength-mismatch, a hard zone near crack for A1-LFW and A3-LFW, on fracture toughness of LFW joint is discussed.

3.1 Hardness distribution near weld interface

Vickers hardness (HV0.2) distributions near the weld on the mid-thickness section were presented in Fig. 7. In A1-LFW, although the maximum temperature was lower than the A_1-transformation temperature, the hardness near the weld interface was higher than that of the base metal far from welds. The maximum hardness at the weld interface for A1-LFW exhibited almost the same as that of A3-LFW. On the other hand, the width of the hard zone for A1-LFW was larger than that of A3-LFW.

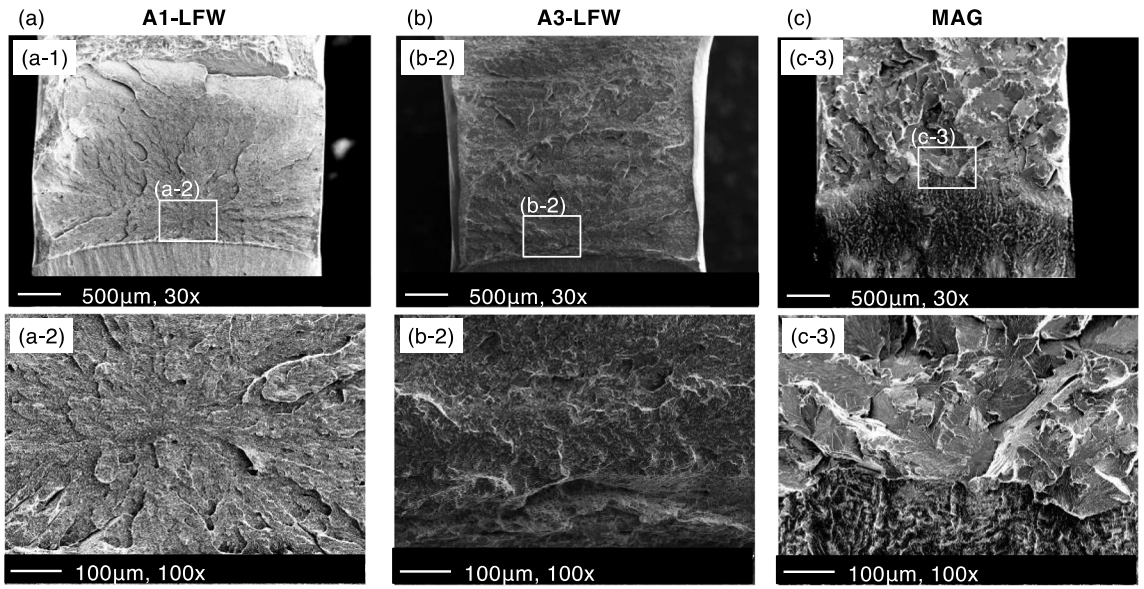

Fig. 5 Fracture appearance of 3 PB specimen in cleavage manner **a** A1-LFW (δ_c = 0.05 mm), **b** A3-LFW (δ_c = 0.36 mm), and **c** MAG (δ_c = 0.01 mm)

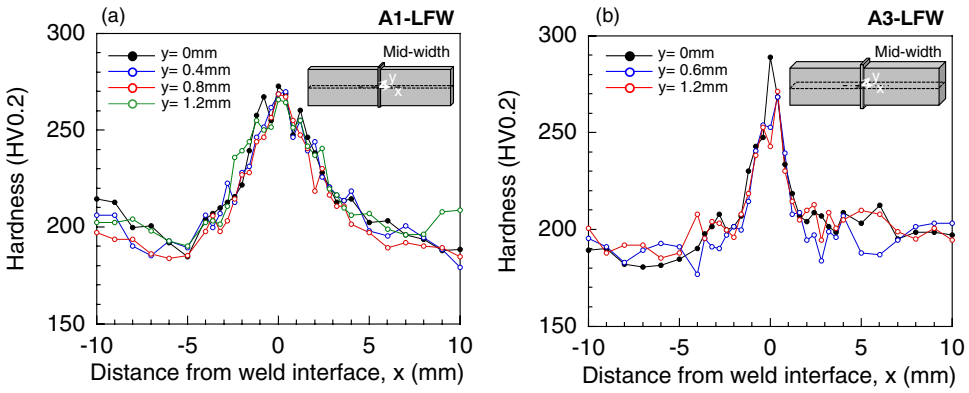

Fig. 7 Hardness distribution near weld interface mid-width section **a** A1-LFW and **b** A3-LFW

3.2 FE-analysis of 3 PB specimen with hard zone near-crack tip

The effect of hard zone width on fracture toughness was discussed by analyzing the stress field near the crack-tip of the 3 PB specimens by elastic–plastic FE-analysis for both A1-LFW and A3-LFW. FE-models were composed of two regions, the base metal (BM) and hard zone (HZ) as shown in Fig. 8. According to the hardness distribution near the weld interface (Fig. 7) in the joint for A1-LFW and A3-LFW, FE-models with of the HZ width $d_{\mathrm{hard}}=4$ mm and 2 mm were assumed, respectively. For comparison, the FE-model (EM: EvenMatch model) composed only of the HZ was also prepared. Crack-tip location was assumed the center in HZ. The elastic–plastic FE analysis was conducted by using the 3-dimensional FE-code, Abaqus 2017. Figure 9 shows the FE models of the 3 PB test specimen used for analysis. The solid elements used were 8-node isoparametric elements with 8 Gaussian points. The minimum element size around the crack-tip was 0.03 mm × 0.03 mm in plane. Equivalent stress—equivalent plastic strain curve of BM at − 50 °C used for FE-analysis was identified by conducting small size round-bar tensile test. Figure 10 shows the true stress—true strain curve of BM obtained by a round-bar tensile test at − 50 °C, and Table 5 summarizes the mechanical properties. Equivalent stress—equivalent plastic strain relationship beyond uniform elongation ε_{T} was constructed by fitting the test data, that is true stress—true plastic strain curve between $3\varepsilon_{\mathrm{T}}/4$ and ε_{T}, with Swift type constitutive equation. Equivalent stress—equivalent plastic strain curve of HZ was assumed by raised toward the larger stress side by the increment of tensile strength, which was estimated from the ratio of the hardness of joint interface to that of BM (see Table 5). Figure 11 presents the identified equivalent stress—equivalent plastic strain curves used for FE-analysis for BM and HZ, respectively.

3.3 The effect of hard zone width on stress field ahead of crack-tip

Figure 12 shows examples of the distributions of the maximum principal stress σ_1 ahead of the crack-tip at mid-thickness for A1-LFW ($d_{\mathrm{hard}}=4$ mm), A3-LFW ($d_{\mathrm{hard}}=2$ mm) and EM at the same CTOD value ($\delta=0.1$ mm). The A1-LFW ($d_{\mathrm{hard}}=4$ mm) presents almost the same maximum principal stress distributions as EM. On the other hand, the A3-LFW ($d_{\mathrm{hard}}=4$ mm) presents significantly lower maximum principal stress distributions than EM. These results indicate that the hard zone for A1-LFW ($d_{\mathrm{hard}}=4$ mm) does not affect stress distribution, but the narrower hard zone for A3-LFW ($d_{\mathrm{hard}}=2$ mm) affects due to plastic constraint loss at this CTOD level. Then, the CTOD levels over which the loss of crack-tip plastic constraint occurs for A1-LFW and A3-LFW were examined. The reference stress σ_{r}, which is defined as the maximum principal stress for each joint at the same location that represents 90% of the peak-stress $\sigma_{1,\mathrm{peak(EM)}}$ ahead of crack-tip (Fig. 12) in EM, are compared as shown in Fig. 13.

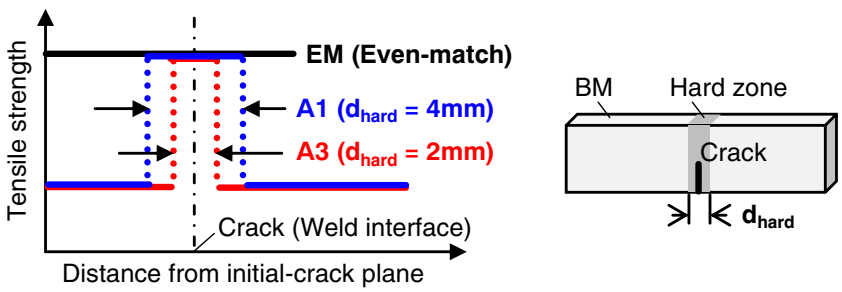

Fig. 8 Hard zone and crack location in FE-analysis

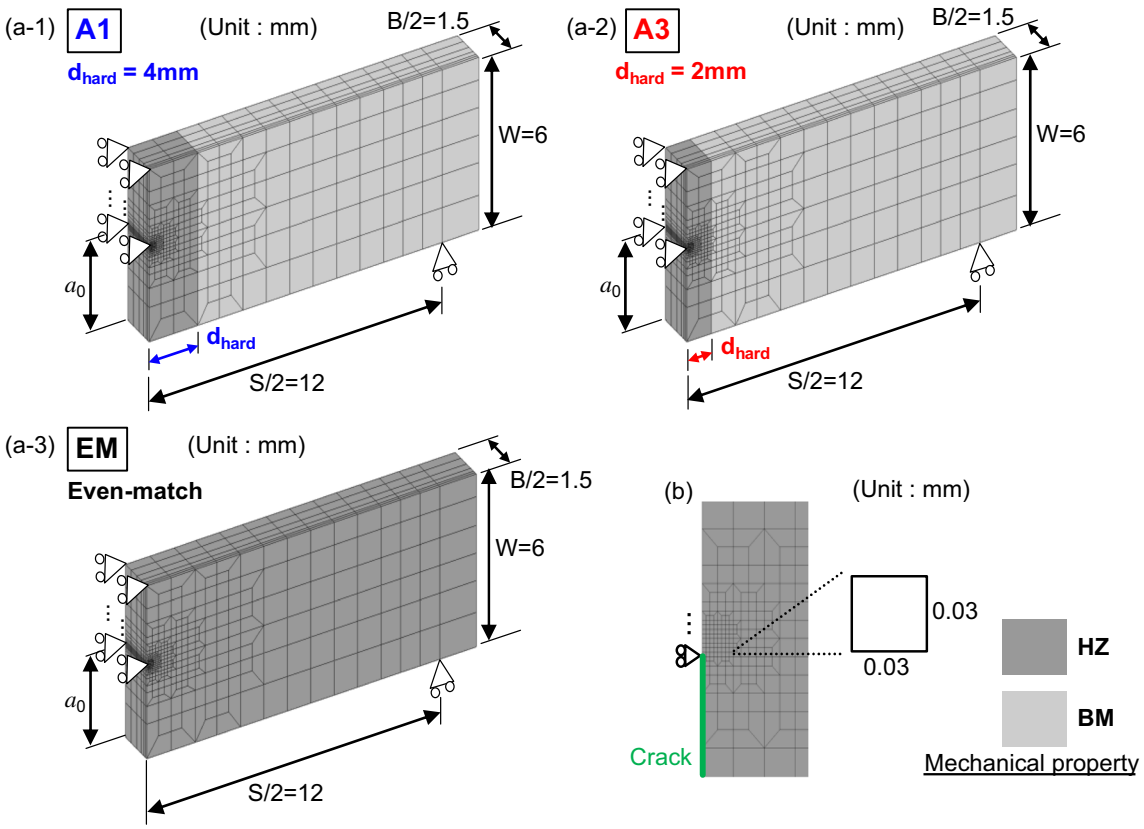

Fig. 9 FE-model used for FE-analysis **a** overview (a-1) A1-LFW, (a-2) A3-LFW, and (a-3) even-match and **b** near crack tip

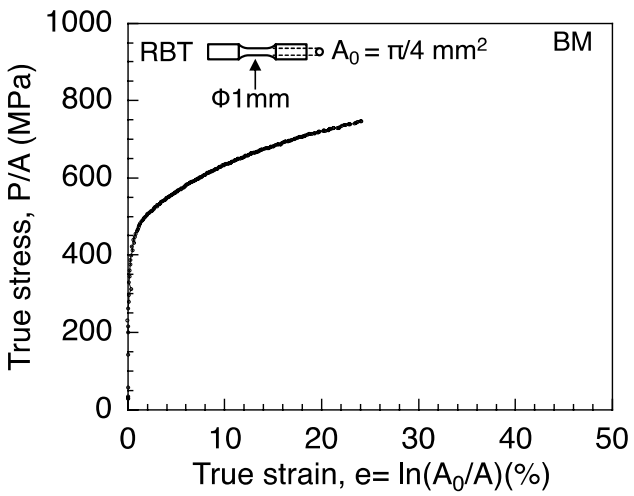

Fig. 10 True stress-true strain curve obtained by smooth RBT specimen of base metal

A1-LFW (d_{hard} = 4mm) presents the same reference stress around the critical CTOD level obtained by experiments (δ_c shown in Fig. 13). This result indicates that the hard zone (d_{hard} = 4 mm) for A1-LFW has no effect on fracture toughness. On the other hand, A3-LFW (d_{hard} = 2 mm) exhibits lower reference stress above a certain CTOD level $\delta \approx 0.01$ mm, which is significantly lower than the critical CTOD level (δ_c shown in Fig. 14). This result implies that the critical CTOD obtained by the test for A3-LFW could be affected by the hard zone (d_{hard} = 2 mm), and could be larger than the intrinsic fracture toughness of the hard zone itself.

Therefore, the critical CTOD obtained by the test for A1-LFW was found to be intrinsic fracture toughness, that was not affected by the hard zone (d_{hard} = 4 mm). On the

Table 5 Mechanical property used for FE-analysis for base metal (BM) and hard zone (HZ)

	$\sigma_{0.2}$ (MPa)	σ_T (MPa)	YR (%)	ε_T (%)
BM	381	591	64.4	0.217
HZ	618	828	74.6	0.217

$\sigma_{0.2}$, 0.2% proof stress; σ_T, tensile strength; *YR*, yield-to-tensile ratio; ε_T, uniform elongation

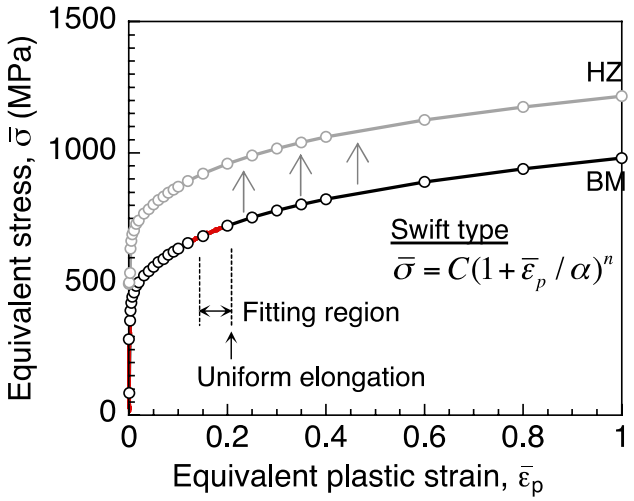

Fig. 11 Equivalent stress-equivalent plastic strain relationship used for FE-analysis

other hand, it was indicated that the critical CTOD obtained by the test for A3-LFW could be higher than the intrinsic fracture toughness due to plastic constraint loss caused by the narrowness of the hardened zone (d_{hard} = 2 mm).

4 Significance of fracture toughness in the view of material at crack-tip

This section discusses the reason why the A1-LFW exhibited lower fracture toughness than BM as well as A3-LFW from metallurgical viewpoints of the joints.

Figure 14 shows the distribution of the nital-etched microstructure on the mid-width section for A1-LFW within 10 mm from the weld center in the forging direction x. Base metal, x = 10 mm away from the weld center, consisted of ferrite and pearlite structure (Fig. 14f). The microstructure

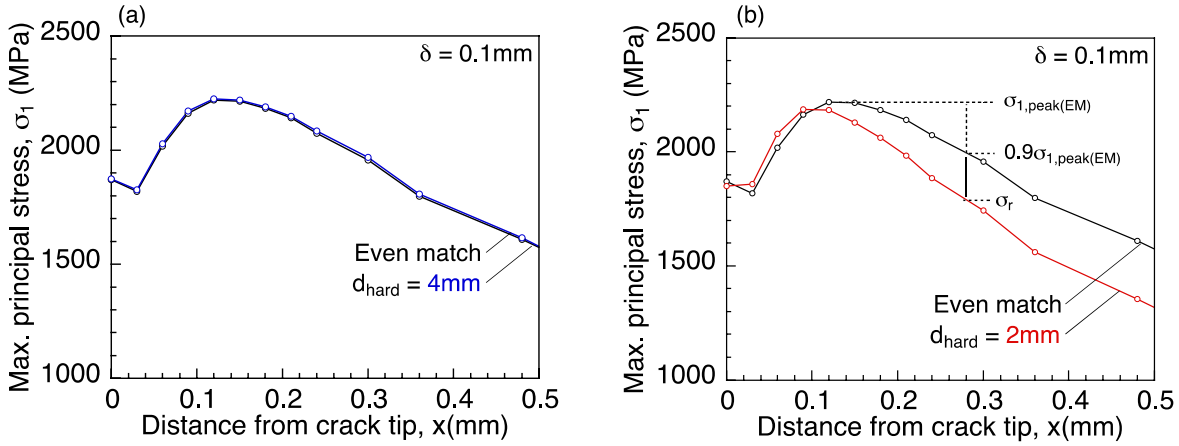

Fig. 12 Equivalent stress-equivalent plastic strain relationship used for FE-analysis **a** A1-LFW (d_{hard} = 4 mm) and **b** A3-LFW (d_{hard} = 2 mm)

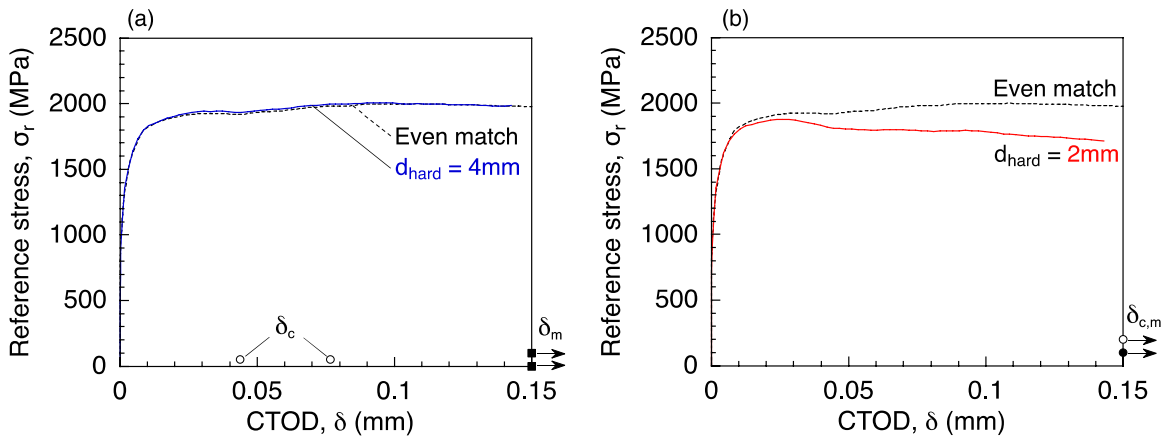

Fig. 13 Effect of deformation level on constraint loss near crack-tip **a** A1-LFW (d_{hard} = 4 mm) and **b** A3-LFW (d_{hard} = 2 mm)

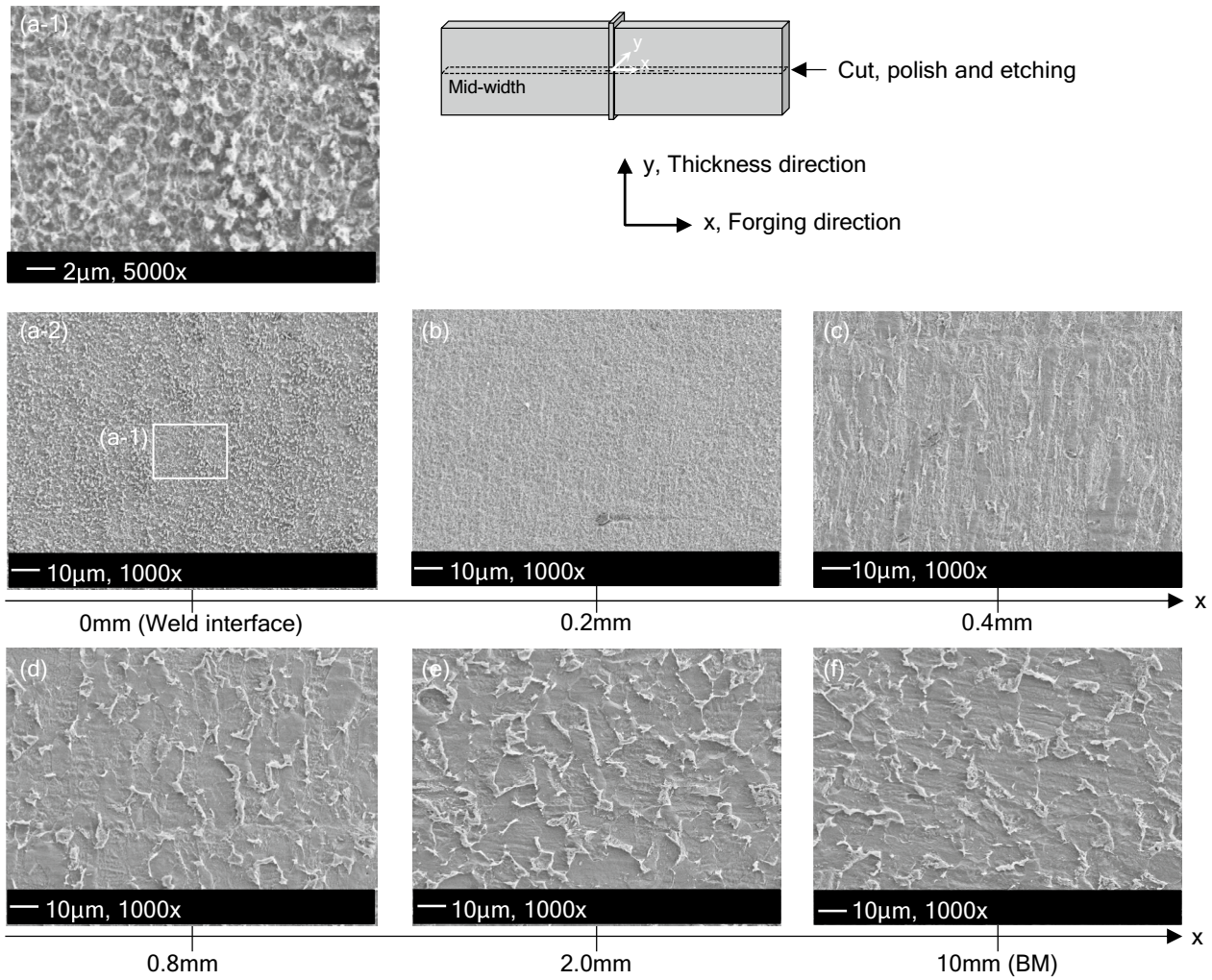

Fig. 14 Nital-etched observation of microstructure near weld interface (A1-LFW) (**a** (1, 2) $x=0$ mm, **b** $x=0.2$ mm, **c** $x=0.4$ mm, **d** $x=0.8$ mm, **e** $x=2.0$ mm, and **f** $x=10$ mm (base metal))

within $x=0.2$ mm away from the weld center exhibited very fine grain (Fig. 14a-1, a-2) in comparison with the base metal. This grain refinement, in a significant narrow region $0 \leq x \leq 0.2$ mm near the weld interface, is presumed to be due to recrystallization, but no grain refinement was observed in the region above $x=0.2$ mm. However, in the region more than $x=0.2$ mm away from the weld center, crystal grains seem to be compressed in the forging direction and a short diameter of the grain in the forging direction gradually changes to the one of base metal ($x=10$ mm). Thus, average short and long diameters of grain L_x and L_y, that is the size in forging and thickness direction, respectively, were measured by using the sectioning method. As shown in Fig. 15, the closer to the weld interface, the smaller grain size in the forging direction L_x within $x=4$ mm away from the weld center was exhibited. From these measurement results, the compressive plastic strain $\bar{\varepsilon}_{p(\mathrm{CP})}$ was calculated by using the following Eq. (1).

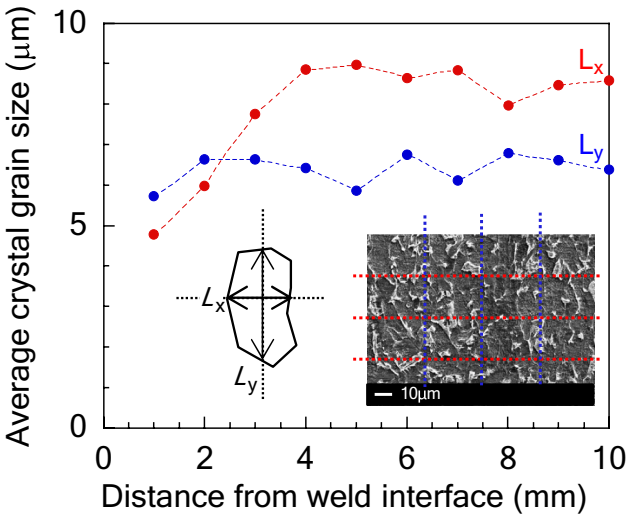

Fig. 15 Distribution of crystal grain size near weld interface (A1-LFW)

$$\epsilon_{p(CP)} = \frac{\sqrt{2}}{3}\sqrt{\left(ln\frac{L_x'}{L_x} - ln\frac{L_y'}{L_y}\right)^2 + \left(ln\frac{L_y'}{L_y} - ln\frac{L_z'}{L_z}\right)^2 + \left(ln\frac{L_z'}{L_z} - ln\frac{L_x'}{L_x}\right)^2} \quad (1)$$

L_x, L_y, and L_z are the undeformed average grain size, and L'_x, L'_y, L'_z are the average grain size deformed in forging, thickness, and oscillation direction, respectively. In addition, $L'_z/L_z = L_xL_y/(L'_xL'_y)$ was used since the volume of grain is assumed constant regardless of applied plastic strain. By this procedure, the distribution of compressive plastic strain was estimated as shown in Fig. 16. The region applied plastic strain above uniform elongation, within $x \leq 2 \sim 3$ mm away from the weld center, presents good agreement with the hard zone (Fig. 7).

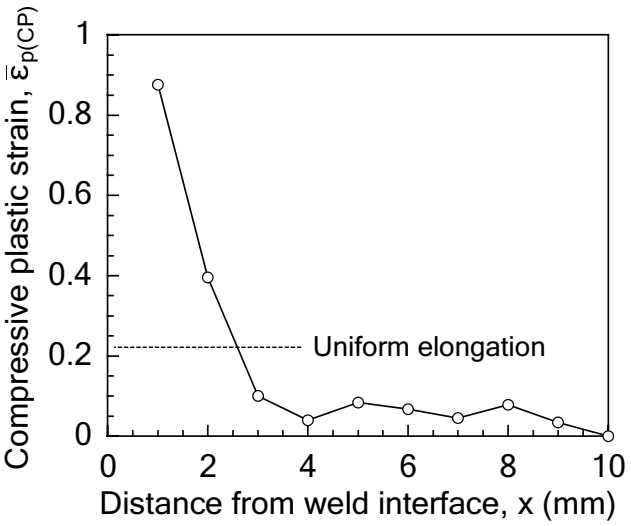

Fig. 16 Distribution of compressive plastic strain near weld interface (A1-LFW)

Furthermore, the ratio of tensile strength, which is assumed to ratio of hardness, on one of the base metals was estimated and compared with experimental results. As shown in Fig. 17a, the true tensile strength $s_{(CP)}$ at each location, where compressive plastic strain was applied above uniform elongation, was estimated by using an equivalent stress-equivalent strain relationship (shown in Fig. 11). Figure 17b shows the estimation of tensile strength normalized by that of base metal $s_{(CP)}/ s_{T(BM)}$ was compared with hardness distribution by mean value of obtained by Vickers hardness test. The ratio of tensile strength estimated from compressive plastic strain presented a good agreement to the ratio of hardness. These results indicate that the hardening near the weld interface except grain refinement could be caused by compressive plastic strain.

The pre-crack for a fracture toughness specimen was introduced toward the center of weld, but the grain refinement was observed to significantly narrow width within $x \leq 0.2$ mm away from the weld center (shown in Fig. 14). Thus, location of cleavage fracture initiation site was analyzed by sectioning observation of specimen fractured in cleavage manner as shown in Fig. 18. The crystal grain size in forging direction directly under fracture initiation site was $L_x = 5.67$ µm (Mean value obtained sectioning method where the distance from

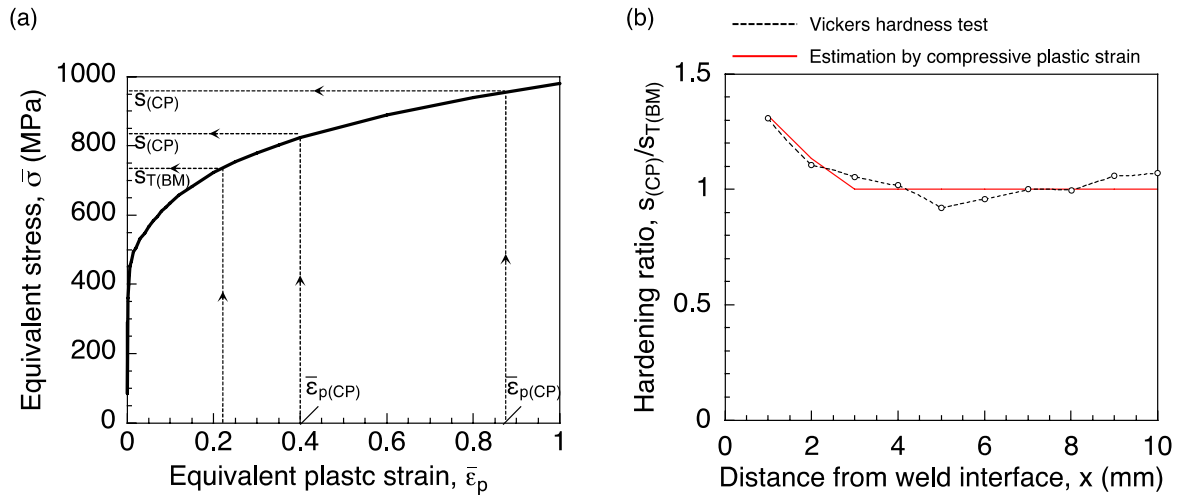

Fig. 17 Hardening due to compressive plastic strain near weld interface (A1-LFW) **a** estimation of strength by means of equivalent stress and **b** comparison of the distribution of hardness ratio estimated with experimental results

fracture surface was 0.12 mm). According to this result and the grain size L_x distribution near the weld interface (Fig. 15), it was indicated that the fracture initiation site was located within $1 \leq x \leq 2$ mm away from the weld center, where no grain refinement occurred but the compressive plastic strain was applied. These results indicated that the critical CTOD value obtained by A1-LFW was fracture toughness for region-affected compressive plastic strain near the weld interface. Therefore, one of the reasons why the fracture toughness for A1-LFW exhibited lower value was found to be hardening and embrittlement due to compressive plastic deformation during LFW process.

For comparison of A1-LFWwith A3-LFW, the distribution of nital-etched microstructure for A3-LFW along the forging direction x of the mid-width section within $x = 10$ mm away from the weld center was also presented in Fig. 19. Base metal, $x = 10$ mm away from the weld center, consisted of ferrite single-phase structure (Fig. 19f). On the other hands, the formation of bainite within $x = 1.0$ mm away from the weld center was observed as shown in Fig. 19a–d. This result confirms that the bainitic transformation occurred weld interface near for A3-LFW. The width where the bainite was for A3-LFW exhibited the good agreement with

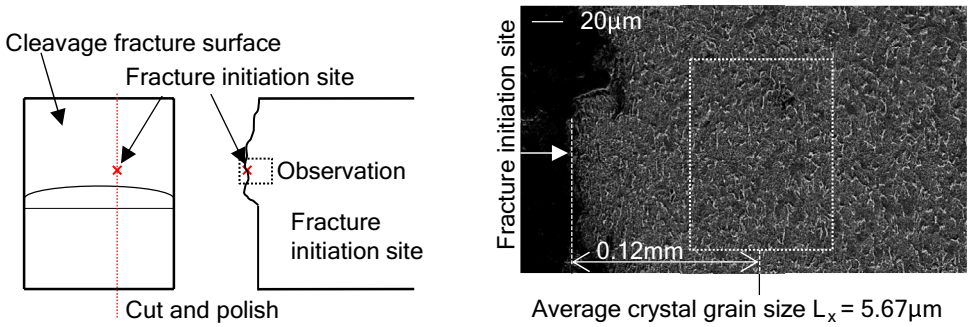

Fig. 18 Identification of crystal grain size directly under fracture initiation site

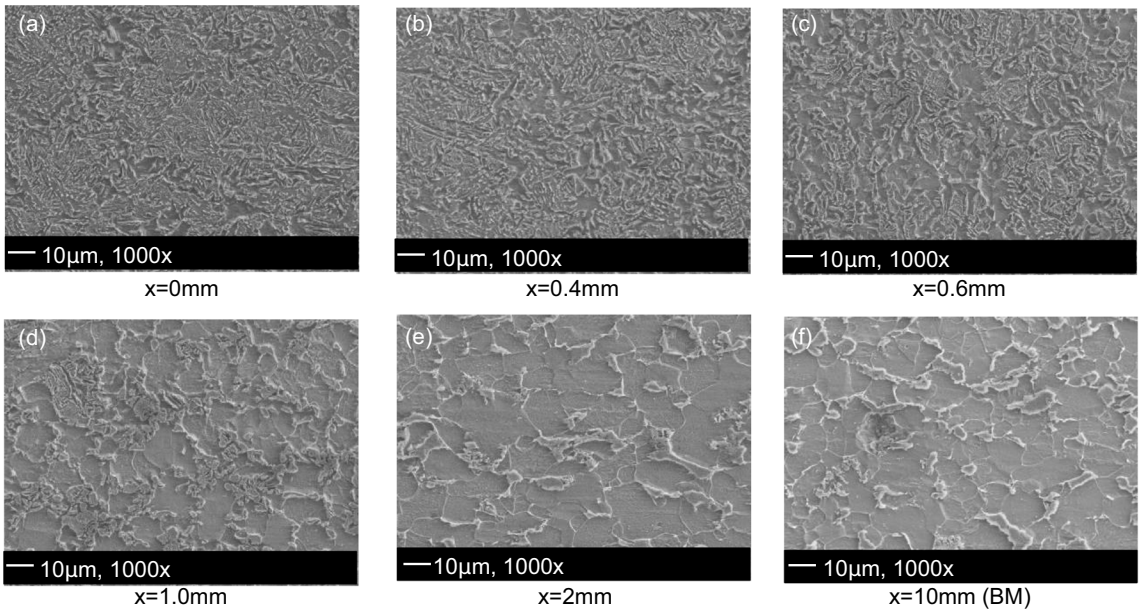

Fig. 19 Nital-etched observation of microstructure near weld interface (A3-LFW) (**a** $x = 0$ mm, **b** $x = 0.4$ mm, **c** $x = 0.6$ mm, **d** $x = 1.0$ mm, **e** $x = 2$ mm, and **f** $x = 10$ mm (base metal))

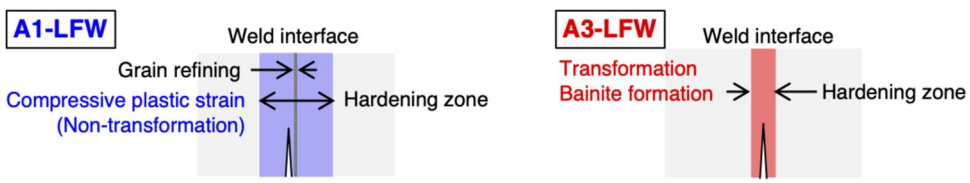

Fig. 20 Schematic illustration of the difference in the mechanism of deterioration of fracture toughness between A1-LFW and A3-LFW

one of the hard zones near the weld interface. Therefore, the fracture toughness for A3-LFW was found to be affected by both of constraint loss due to hardening and the bainitic transformation.

According to these observation and analysis, the characteristics to affect fracture toughness near the weld interface were considered schematically shown in Fig. 20. The fracture toughness of the weld joint for A1-LFW deteriorated due to not transformation but compressive plastic deformation, where the metal heated under A1-temperature was not completely ejected by friction but remained around the joint interface. On the other hand, fracture toughness for A3-LFW could be reduced due to bainite formation near the weld interface, although that presented an apparently higher value than the toughness affected by constraint loss near crack in narrow hard zone. In addition, it is implied that the metal heated above A3 temperature was completely ejected by friction under lower compressive pressure. These results also indicated that it is desirable to control the condition for LFW process so that the hard zone to be as narrow as possible in case of inevitable hardening near weld interface.

5 Conclusion

Two types of LFW joint of weathering steel SPA-H, whose maximum temperature in weld joint during LFW process was controlled to be lower than the A_1-transformation temperature (A1-LFW) and higher than the A_3-transformation temperature (A3-LFW), were subjected to fracture toughness test. Both A1-LFW and A3-LFW exhibited higher critical CTOD than that of the heat-affected zone of MAG welds for the same steel. Therefore, the LFW was found to be more effective for the joining of weathering steel compared with conventional arc welding in terms of fracture toughness. However, A1-LFW exhibited lower fracture toughness (critical CTOD) than that of base metal or A3-LFW.

The significance of the test results was discussed from mechanical and metallurgical viewpoints. As the results of FE-analysis assuming strength mismatch according to hardness in the joint, the hard zone whose width was relatively large ($0 \le x \le 2$ mm away from the weld center, $d_{hard} = 4$ mm) was found to have no effect on the stress field near crack tip. This result indicated that the critical CTOD obtained by the test for A1-LFW was the intrinsic fracture toughness of the hard zone itself. The fracture initiation site was found to locate within $1 \le x \le 2$ mm away from the weld center, where no grain refinement occurred but compressive plastic strain was applied. Therefore, the fracture toughness for A1-LFW was found to be deteriorated due to work hardening associated with compressive plastic straining during LFW under higher compressive pressure.

On the other hand, the deterioration of fracture toughness for A3-LFW was found to be caused by hardening due to bainitic transformation near the joint interface. However, the FE-analysis of the stress field near the crack-tip indicated that the critical CTOD obtained by the test for A3-LFW could be affected by the hard zone whose width was relatively narrow ($0 \le x \le 1$ mm away from the weld center, $d_{hard} = 2$ mm). This analytical result means that the narrowness of the hardened region provided a little bit higher toughness than the intrinsic fracture toughness of the transformed phase due to plastic constraint loss. From these results, it was also found to be desirable to control the condition for LFW process so as the hardened region to be narrow in case of inevitable deterioration due to hardening near the weld interface.

Acknowledgements The authors appreciate the financial support of the ISIJ Research Project of The Iron and Steel Institute of Japan.

Funding Open Access funding provided by Osaka University. Partial financial support was received from the ISIJ Research Project of The Iron and Steel Institute of Japan.

Data Availability The data that support the findings of this study are available from the corresponding author, K. Shimizu, upon reasonable request.

Declarations

Competing interests The authors declare no competing interests.

References

1. Richter W (1929) Creation of an adhesive bond between plaques of tool steel and their supports in the manner of welding or soldering, Germany patent DE477084
2. Vairis A, Frost M (1998) High frequency linear friction welding of a titanium alloy. Wear 217(1):117–131. https://doi.org/10.1016/S0043-1648(98)00145-8
3. Wanjara P, Jahazi M (2005) Linear friction welding of Ti-6Al-4V: processing, microstructure, and mechanical-property interrelationships. Metall and Mater Trans A 36(8):2149–2164. https://doi.org/10.1007/s11661-005-0335-5

4. Mary C, Jahazi M (2008) Multi-scale analysis of IN-718 microstructure evolution during linear friction welding. Adv Eng Mater 10(6):573–578. https://doi.org/10.1002/adem.200700361
5. Aoki Y, Kuroiwa R, Fujii H, Murayama G, Yasuyama M (2019) Linear friction stir welding of medium carbon steel at low temperature. ISIJ Int 59(10):1853–1859. https://doi.org/10.2355/isijinternational.ISIJINT-2018-458
6. Kuroiwa R, Liu H, Aoki Y, Yoon S, Fujii H, Murayama G, Yasuyama M (2020) Microstructure control of medium carbon steel joints by low-temperature linear friction welding. Sci Technol Weld Joining 25(1):1–9. https://doi.org/10.2355/isijinternational.ISIJINT-2018-458
7. Choi JW, Li W, Ushioda K, Yamamoto M, Fujii H (2022) Strengthening mechanism of high-pressure linear friction welded AA7075-T6 joint. Mater Charact 191:112112. https://doi.org/10.1016/j.matchar.2022.112112
8. Stinville JC, Bridier F, Ponsen D, Wanjara P, Bocher P (2015) High and low cycle fatigue behavior of linear friction welded Ti–6Al–4V. Int J Fatigue 70:278–288. https://doi.org/10.1016/j.ijfatigue.2014.10.002
9. Owsiński R, Lachowicz DS, Lachowicz CT, Gil R, Niesłony A (2021) Characterisation of joint properties through spatial mapping of cracks in fatigue specimens, extracted from the linearly friction welded steel coupon. Precis Eng 71:78–89. https://doi.org/10.1016/j.ijfatigue.2014.10.002
10. Wang Y, Tsutsumi S, Kawakubo T, Fujii H (2022) Microstructure, mechanical properties and fatigue behaviors of linear friction welded weathering steels. Int J Fatigue 159:106829. https://doi.org/10.1016/j.ijfatigue.2022.106829
11. Miao H, Tsutsumi S, Yamashita T, Morisada Y, Fujii H (2023) Fatigue strength improvement of linear friction welded butt joints of low carbon steel by pressurizing after oscillation. J Manuf Process 102:795–805. https://doi.org/10.1016/j.jmapro.2023.08.004
12. Ma TJ, Li WY, Yang SY (2009) Impact toughness and fracture analysis of linear friction welded Ti–6Al–4V alloy joints. Mater Des 30(6):2128–2132. https://doi.org/10.1016/j.matdes.2008.08.029
13. Zhao P, Wei C, Li Y, Tao J, Zhang C, Xiao X, Zhang M (2021) Effect of heat treatment on the microstructure, microhardness and impact toughness of TC11 and TC17 linear friction welded joint. Mater Sci Eng, A 803:140496. https://doi.org/10.1016/j.matchar.2022.112112
14. Minami F, Toyoda M, Thaulow C, Hauge M (1995) Effect of strength mis-match on fracture mechanical behavior of HAZ-notched weld joint. Quart J Japan Weld Soc 13(4):508–517. https://doi.org/10.2207/qjjws.13.508
15. Kawabata T, Sakaibori H, Onishi K, Mochizuki M, Okano S, Kitano H (2010) Effect of undermatched joint on brittle fracture behavior of high strength steel plate. Quart J Japan Weld Soc 28:296–304. https://doi.org/10.2207/qjjws.28.296
16. Shi Y, Han Z, Fu J (1998) Effects of weld strength undermatch on fracture toughness of HAZ notched weldments in a HSLA steel. Int J Fract 91(4):349–358. https://doi.org/10.1023/A:1007411221854
17. Minami F, Nakano Y, Suzuki S, Shiwaku T, Moriya Y, Hagiwara Y, Toyoda M (1994) Fracture toughness evaluation of multipass weld HAZ with focus on mechanical mis-matching effect. Quart J Japan Weld Soc 12(4):568–574. https://doi.org/10.2207/qjjws.12.568
18. Minami F, Nakano Y, Suzuki S, Shiwaku T, Moriya Y, Hagiwara Y, Toyoda M (1995) Fracture toughness evaluation of multipass weld HAZ considering the strength mismatch effect. Weld Int 9(7):546–553. https://doi.org/10.1080/09507119509548849
19. Walter NMV, Lemos GVB, Kieckow GS, Buzzatti DT, Buzzatti JT, Mattei F, Reguly A, Clarke T, Paes MTP, Dalpiaz G, Marinho RR (2024) Investigating microstructure, mechanical properties, and pitting corrosion resistance of UNS S32760 super duplex stainless steel after linear friction welding. J Market Res 31:1637–1643. https://doi.org/10.1016/j.jmrt.2024.06.191
20. ISO12135: 2021 (2021) Metallic material− unified method of test for the determination of quasistatic fracture toughness Status. https://ndlsearch.ndl.go.jp/books/R100000136-I15719800754365 90208
21. WES1108:2015 (2015) Standard test method for crack-tip opening displacement (CTOD) fracture toughness measurement. https://www-it.jwes.or.jp/wes_ki/wes.jsp